e-PS, 2005, **2**, 19-29
ISSN: 1581-9280

www.e-PreservationScience.org
www.Morana-rtd.com

e-PRESERVATIONScience
published by MORANA RTD d.o.o.

FULL PAPER

REVIEW

SHORT COMMUNICATION

DEGRADATION OF LIME WOOD PAINTING SUPPORTS

CARMEN - MIHAELA POPESCU[1,2], YUSAKU SAKATA[2], MARIA - CRISTINA POPESCU[1], AKIOSHI OSAKA[3] AND CORNELIA VASILE[1*]

1. Romanian Academy, P. Poni Institute of Macromolecular Chemistry, Department of Physical Chemistry of Polymers, 41A Gr. Ghica Voda Alley, 700487 Iasi, Romania

2. Department of Applied Chemistry, Faculty of Engineering, Okayama University, Japan

3. Biomaterials Laboratory, Faculty of Engineering, Okayama University, Japan

*corresponding author: cvasile@icmpp.ro

Abstract

Degradation of wood, being a natural process, leads to destruction of wooden objects of historic and cultural value, resulting in loss of cultural heritage. Wood can survive centuries or even thousands of years, if kept in an environment, which limits microbial activity. In an unfavourable environment physical, chemical and morphological modifications of wood also take place as a result of biodegradation. It is important to know the type of degradation and how the processes influence material properties if wooden items are to be properly preserved.

The objective of this study is to present new knowledge on non-invasive techniques useful to assess the preservation status of lime wood in art objects. The methods of investigation were optical and electronic microscopy, wide angle X-ray scattering (WAXS), and FT-IR spectroscopy.

Following a deconvolution process of the diffraction patterns, crystalline index, apparent lateral crystallite size, proportion of crystallite interior chains, orientation index, mesomorphism, cellulose fraction have been determined and shown to change with increasing age of painting supports. Structural modifications were assessed by FT-IR spectrometry and 2D correlation FT-IR spectroscopy, while morphological modification were characterised using SEM. The principal hetero-elements of the lime wood samples were detected by EDX. It can be concluded that only a multi-analytical approach can provide the information needed on wood degradation processes.

received: 18.05.2005
accepted: 14.09.2005

key words:
lime wood, degradation, conservation, spectroscopy, microscopy, WAXS, FT-IR

1. Introduction

Throughout the history, many art objects have experienced changing fortunes: periods of splendour and recognition associated with careful handling, as well as disasters such as wars, fires and floods, followed by periods of inadequate storage. Wooden cultural heritage can be further degraded by micro-organisms, if moisture, oxygen and other environmental factors are favourable for microbial growth.[1] Additionally, there are a number of environmental (non-biological)

Sample	Description and origin	Preservation status	Tree age (year)	Sample age (year)
A	Lime-tree panel – non-degraded	Excellent	70	~6
B	Lime wood support of iconostasis, "St. Imp. Constantin and Elena" church from Iasi (~1900)	Unstable (active biological attack)	85	~100
C	Putna Monastery Lime wood iconostasis (~1730), undergone a conservation treatment	Unstable (biological attack stopped)	72	~270

Table 1. Provenance, qualitative observation on the preservation status, and dendrological characteristics of the lime wood samples used in the study. Collected in collaboration with the Academy of Fine Art and Fine Art Museum of Iasi.

parameters that contribute significantly to the degradation of wood, including humidity, temperature, solar irradiation, atmospheric ozone, and pollution.[2]

Wooden objects exposed to humid conditions (temporarily or permanently) are subject to microbial deterioration.[3] Both heterotrophic and autotrophic microorganisms participate in these processes. The composition of the microbiota that develop on a historic object is largely determined by the availability of moisture. The changes caused by microorganisms are associated with enzymatic degradation or excretion of various metabolic products. The main causes of these effects are *Actinomycetes* and microscopic fungi, while *Eubacteria* and wood-rot fungi present a particular hazard to wooden objects.

While brown-rot fungi selectively decompose structural carbohydrates, lignin degradation is limited, which is why this component gradually becomes more and more prominent in brown-rotted wood. White-rot fungi decompose all structural cell wall constituents, although the rate at which they do this differs. Selective (or preferential) white-rots decompose hemicellulose and lignin first, resulting in defibrillation through dissolution of the middle lamella. In contrast, non-selective (or simultaneous) white-rots remove lignin and structural carbohydrates at a similar rate, resulting in homogeneous cell wall decay.

Our previous studies[4,5] were focussed on changes in chemical composition. The preservation status and dendrochronological characteristics were shown to correlate with variations in elemental composition (C, H, O, N) of ash, and with the pH and moisture content of the sample. In order to characterise the degradation processes, physical, structural and chemical changes occurring under the influence of the environment have been correlated with thermogravimetric data. It has been established that thermal characteristics of the process of elimination of adsorbed water depend on sample age and on the applied conservation treatments.

The objective of the present study is to investigate non-invasive methods to be used for assessing the age and preservation status of lime wood (softwood) supports from art works (paintings, decorations, ornaments, etc.) as a part of a larger study on the ageing of softwood-based cultural heritage.

2. Experimental

2.1 Materials

In comparison to other soft woods, wood of lime trees (*Tillia cordata* P. Mill.) found widespread use in panel painting and polychrome sculpture techniques. In our study, we used soft lime wood from supports of old paintings (icons and iconostasis), which was 100–300 years old. A new sample of non-degraded wood was taken as reference. However, it has to be stressed that the preservation status of a sample is not a consequence of aging as such, but of biological attack. Conversely, sample age may not correlate with the preservation status.

Both the reference and the old samples were first dendrochronologically characterised, the results are presented in Table 1.

2.2 Methods

Characterisation and analysis of artworks should preferably be done using non-invasive, non-destructive methods. In some cases, micro-samples (a few milligrams) are allowed to be taken, however, using these samples, separation of the main components of wood and their subsequent characterization is not possible. As the investigation is thus limited to the sample as a whole, the interpretation of experimental data is difficult.

The diffraction experiments yield information on the nanometre level, while scanning procedures provide resolution, which is defined by the X-ray beam diameter, usually in the micrometer range. Structures to about a micrometer in size are accessible to light microscopy, higher resolution can be achieved using other methods, such as scanning-electron microscopy. Electron microscopy and X-ray diffraction are ideal tools for characterisation of fibre orientation (texture) and the size and arrangement of the components in the nanocomposites.

Electron microscopy (SEM) has the disadvantage

of requiring a pre-treatment of the sample, which is absent in the WAXS scattering technique. Obtaining good statistics for fibril diameter is another difficulty associated with SEM, because a high number of pictures have to be evaluated quantitatively. On the other hand, scattering methods provide averages over the structures inside a macroscopic sample volume, e.g. a cubic millimetre. The main drawback of WAXS is that it is an indirect method and that one has to rely on models to evaluate the data. Moreover, the width of Bragg peaks in X-ray scattering depends not only on the size of the crystalline regions but also on how perfect they are, which has to be considered carefully when interpreting WAXS results.

Lime wood slices were cut along the longitudinal direction of the stem. Since scattering measurements do not require any chemical and physical treatment, the wood samples were investigated in their natural state. For WAXS and SEM investigations, air dried samples with a water content determined by TG/DTG measurements of 8.3% - 8.7%.

2.2.1 Microscopy

IOR MC1 optical microscope at room temperature has been used at magnification x360. Longitudinal and cross sections were examined.

2.2.2 SEM-EDX analysis

The lime wood samples were analysed with a Scanning Electron Microscope (SEM, JEOL, JMS-6300) equipped with an energy-dispersive X-ray analyser (EDX-4, Phillips). The acceleration voltage was 20 kV and the current of electron beam 300 mA. Samples were coated with carbon.

2.2.3 X-ray diffraction

Wide angle region WAXS for scattering angle of $2\theta > 2^{o}$ was used to determine dimensions of the unit cell and distances in real space <10 Ĺ and crystallographic aspects such as lattice spacing, average crystallite size, degree of crystallinity and preferred crystallographic orientation.

Small pieces of thickness less than 1 mm were used, arranged in parallel with the fibre axis. The X-ray diffractograms were recorded on XRD equipment Rigaku 2050/32 by Rigaku Co. Japan. This device was used to determine the crystallinity of cellulose. The samples were arranged longitudinally to the direction of stem. The measurements were carried out in point focus geometry using Cu K_{α} radiation λ = 0.1524 nm. Experimental conditions: sequence scan mode; measuring axis: $2\theta/\theta$; voltage: 40 kV; current: 20 mA; start angle: 10^{o}; stop angle: 80^{o}; sampling angle: 0.021^{o}; scan rate of goniometer: 2^{o}/ min; divergent slit width: 1^{o}; receiving slit width: 1^{o}; scattering slit width: 0.60 mm; monochromator receiving slit width: 0.80 mm. All the measurements were conducted in diffraction mode in air atmosphere (pressure).

2.2.4 FTIR spectrometry

Transmittance FT-IR spectra were measured using the KBr pellet technique. The samples were removed from wood surfaces and mixed with KBr (for IR spectroscopy, Merck), content of sample 1.2% (w/w). Dust samples were sieved and fractions with the diameter less than 0.2 mm were retained for analysis. The spectra represent averages of five.

Bomem MB-104 spectrometer with a resolution of 4 cm-1 and 100 scans were taken per sample. Processing of the spectra and baseline correction was done by means of Grams/32 program (Galactic Industry Corp.). Peak height and area values for lignin associated bands were determined against carbohydrate reference peaks to provide relative changes in the composition of the structural components.

2.2.5 2D correlation IR spectroscopy

Two-dimensional (2D) correlation spectroscopy is a mathematical tool whereby a cross-correlation analysis is applied to sinusoidally varying dynamic IR signals to construct a set of 2D IR correlation spectra.[6,7] Generalized 2D correlation spectroscopy, which is an extension of original 2D correlation spectroscopy, allows one to apply a variety of perturbations to generate 2D correlation spectra of the analyzed system.[8] However, the 2D correlation spectroscopy relies on the resolution of the original spectra.

By spreading peaks along the second dimension, 2D correlation spectroscopy sort out complex or overlapped spectral feature and enhances spectral resolution.[9] 2D FTIR correlation intensities were calculated using a MATLAB programme using the generalized 2D correlation method developed by Noda.[8] For all calculations, the first spectrum was used as reference spectrum. In 2D correlation analysis, two kinds of correlation maps (synchronous and asynchronous) are generated from a set of dynamic spectra obtained from the modulation experiment.[8] Synchronous 2D-correlation spectra represent the simultaneous or coincidental changes of spectral intensities measured at the wavenumbers ν_1 and ν_2. Correlation peaks appearing at the diagonal position ($\nu_1 = \nu_2$) correspond to the linear evolution of a given species along the induced perturbation, i.e. auto-peaks. On the other hand, correlation peaks appearing out of the diagonal position ($\nu_1 \neq \nu_2$) correspond to simultaneous changes of spectral signals at two different wavenumbers, which

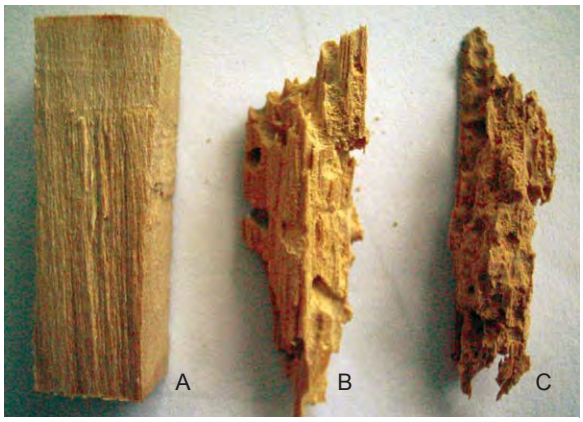

Figure 1. Visual observation of the advancing decay of lime wood

may be positively or negatively correlated with each other. An asynchronous correlation peak develops only if the intensities of the two dynamic spectral intensities vary out of phase (delayed or accelerated).

3. Results and Discussion

3.1 Visual observation

The visual consequences of advancing degradation of lime wood are shown in Figure 1. The state after 270 years appears structurally very weak. In the case of lime wood approx. 100 years old, the xylophagous attack is not as advanced and its structure is more compact.

3.2 Examination using microscopy

At the microscopic level (Figures 2 and 3) the degradation is evident in that fibrils gradually become more disrupted.

In the cross section, the thick-walled vessels appear ordered in the non-degraded sample (Figure 3A) while in degraded wood there are regions where they are disordered, destroyed and of increased dimensions (Figures 3B and 3C).

The SEM micrographs were taken at a different magnification (x250, x1000) in longitudinal direction of the stem. Structural differences can be observed according to the age of sample. Lime wood, similar to other softwoods, is composed of overlapping vessels, connected by bordered pit apertures, and parenchyma cells (Figure 5A). The non-degraded wood fibrils are smooth and uniform. In the lime wood sample aged 100 years, defibrilation is evident and the vessels become disconnected, and after an even longer period, some fibrils/vessels are broken (Figure 4C). Even the inner structure of some fibrils/vessels is destroyed (Figure 5C).

The diameter of morphological entities decreases from ~50 μm for non-degraded wood to 42 ± 4 μm and 36 ± 4 μm for samples B and C, respectively. The images indicate a progressive erosion of the cell wall. According to the literature this occurs when components are degraded simultaneously or a diffuse attack on lignin may occur by a microorganism that preferentially removes lignin.[1,3,10,11] Cell wall carbohydrates are degraded extensively during the decay, leaving a modified, lignin-rich substrate, which degrades at a different rate, possibly under the influence of different microorganisms.

The percentage of main elements present in wood samples determined by SEM/EDX analysis is given in Table 2. The changes in the composition

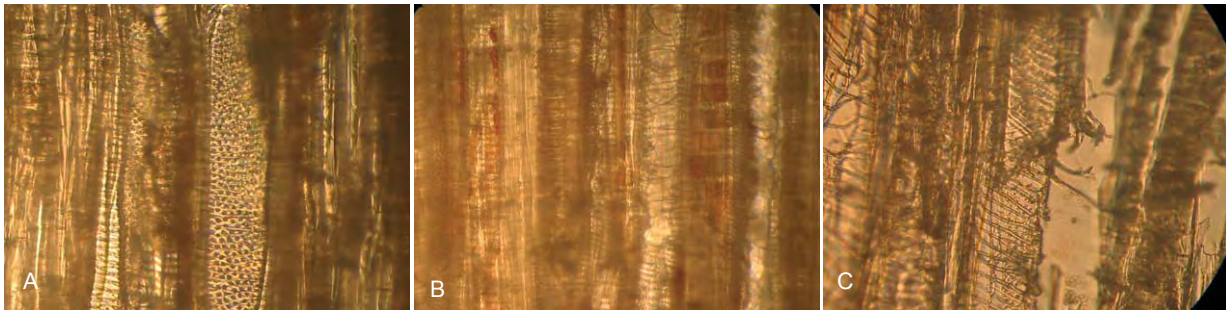

Figure 2. Images of lime wood samples in longitudinal direction at a magnification of x360.

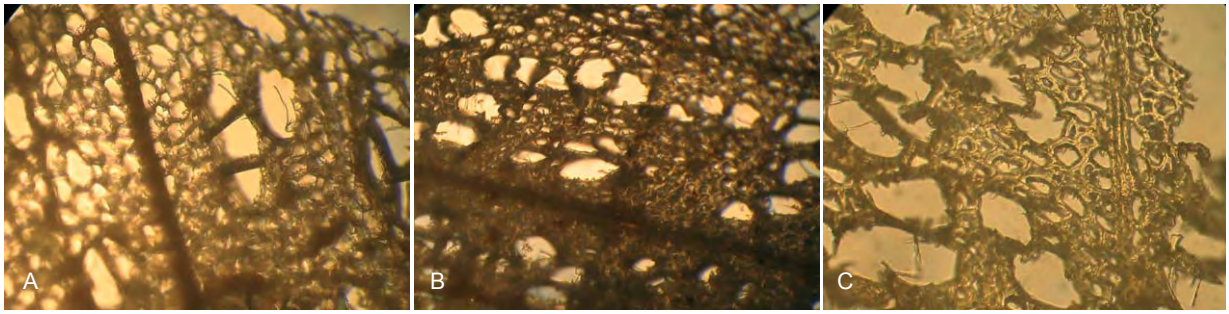

Figure 3. Images of lime wood samples in cross section at a magnification of x360.

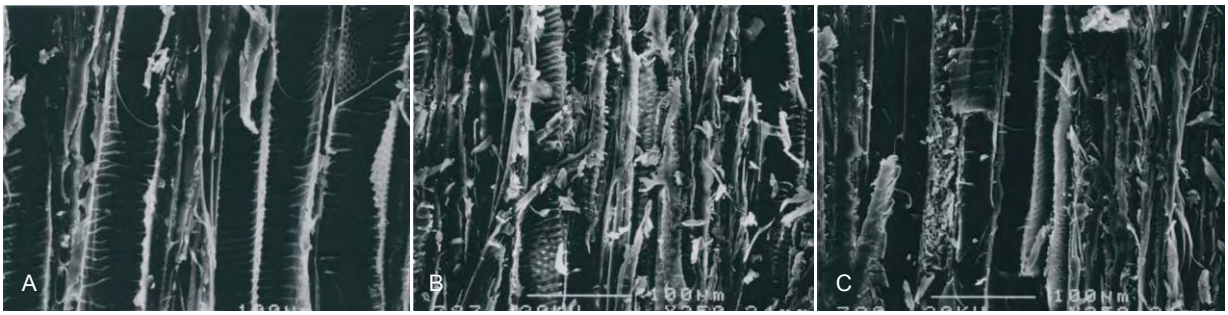

Figure 4. SEM micrographs of lime wood samples at a magnification of x250.

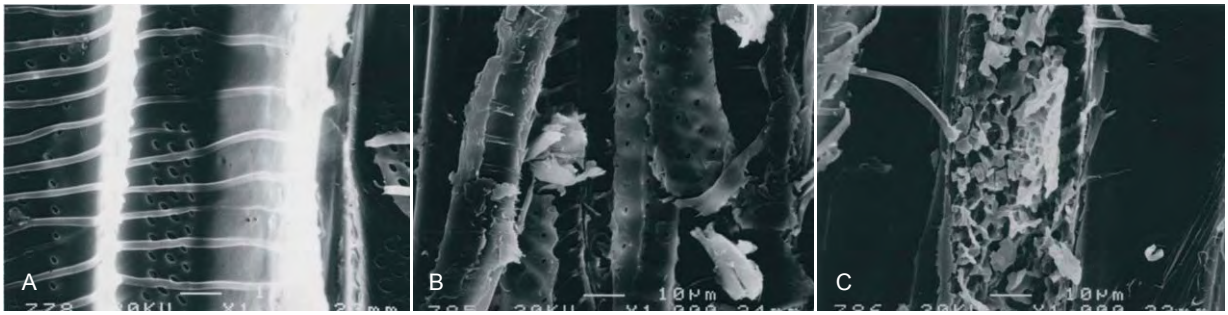

Figure 5. SEM micrographs of lime wood samples at a magnification of x1000.

Sample	O (%)	Na (%)	Si (%)	P (%)	Mo (%)	Cl (%)	K (%)	Ca (%)
A	89.4	3.84	0.40	1.05	0.50	1.52	1.22	2.12
B	87.1	6.76	0.65	0.10	0.60	1.60	1.12	2.04
C	88.7	-	0.50	-	-	0.60	0.40	6.02

Table 2. Principal elemental composition of lime wood samples.

are small and should not influence interpretation of XRD spectra.

3.3 Examinations using WAXS

Figure 6 shows the X-ray diffractograms of the lime wood samples. The WAXS peaks at 2θ = 15° and 16.5° merged into a broad band, which is consistent with the literature.[12,13] The most prominent peak was 2θ = 22.4° and it was used in our evaluations. This peak is assigned to (200) plane, which is not parallel to any face. The X-ray diffraction pattern of wood is mainly that of cellulose.

In order to examine the intensities of diffraction bands and to establish the crystalline and the amorphous areas more exactly, the diffractograms were deconvoluted using Gaussian and mixed Gaussian-Lorenzian profiles (Figure 6). The positions of peaks of the cellulose crystalline form I,[14] were found not to be significantly different in undegraded and degraded lime wood samples.

After the deconvolution, five bands can be observed, namely: (2θ) reflection at 15° assigned to the (101) crystallographic plane, the 16.5° (2θ) reflection, assigned to the (10Î) crystallographic plane, the 18.9° (2θ) reflection, assigned to amorphous phases, the 20.4° (2θ) reflection, assigned to the (012) crystallographic plane, and the 22.4° (2θ) reflection, assigned to the (002) or (200) crystallographic plane of cellulose I.[2,13,15-20]

The peak at 2θ = 22.4° decreases with degradation while the peak at 2θ = 20.4°, has a tendency to increase, and similar behaviour is evident for the peak for the (101) plane 2θ = 15.03°. The peaks at 2θ = 15.03° and 16.5° become better separated with sample age. Crucial for the analysis of XRD data is the separation of the reflection (002) from the amorphous background and the reflections (012), (101) and (10Î). After deconvolution, several parameters can be calculated and compared,[16,17,18] e.g. the crystalline index, pro-

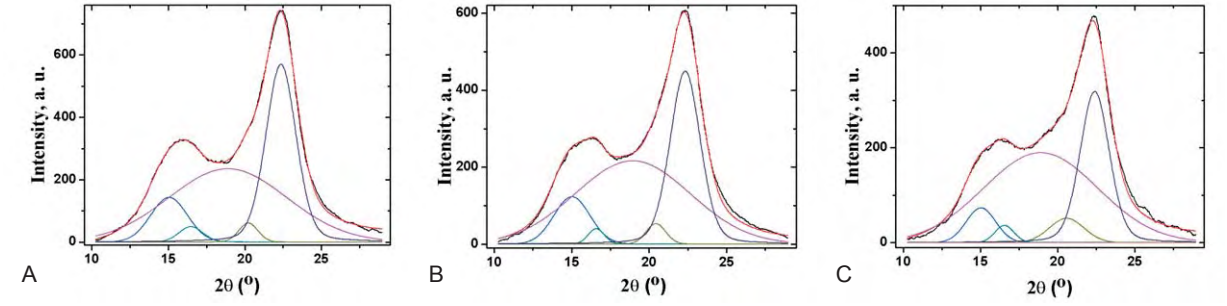

Figure 6. Deconvoluted diffractograms of lime wood samples.

posed by Hermans[18]

$$\mathrm{Cr.I.} = \frac{A_{\mathrm{crist}}}{A_{\mathrm{total}}} \quad ,(1)$$

where: Cr.I. is the crystalline index, A_{crist} is the sum of peak areas (101), (10Î), (002) and (012), and A_{total} is the total area under diffractogram. Vuorinen and Visapä[19] and Segal[23] used intensity data:

$$\mathrm{Cr.I.}' = 1 - \frac{I_{\mathrm{am}}}{I_{002}} \quad ,(2)$$

where: I_{002} is the maximum intensity of the (002) lattice diffraction, I_{am} is the intensity diffraction of the amorphous band. The apparent crystallite size was estimated through the use of the Scherrer equation:[2,16,17-21,24]

$$L = \frac{K \cdot \lambda}{\beta \cdot \cos\theta} \quad ,(3)$$

where K is a constant with the value of 0.94, λ is the X–ray wavelength (0.1542 nm for Cu K_α radiation), β is the half-height width of diffraction peak and θ is the Bragg angle corresponding to the (002), (101) or (10Î) plane. The surface chains occupy a layer approximately 0.57 nm thick, so the proportion of crystallite interior chains is:[21]

$$X = \frac{(L - 1.14)^2}{L^2} \quad ,(4)$$

where: L is the apparent crystallite size for the (002) reflection. The orientation index was estimated using the equation:[17]

$$\mathrm{O.I.} = \left(1 - \frac{I_{\mathrm{am}}}{I_{\mathrm{tot}}}\right) \quad ,(5)$$

where: I_{tot} is the maximum intensity of the diffraction pattern. Lateral orientation was calculated according to:[17]

$$\mathrm{L.O.} = \left(1 - \frac{I_1}{I_2}\right) \cdot 100 \quad ,(6)$$

where I_1 is the intensity of the higher of the two crystalline bands (at 16.5 and 18.9°) and I_2 is the band height at 15°. Mesomorphysm was calculated according to[17]:

$$\mathrm{Mm} = (\mathrm{O.I.} - \mathrm{Cr.I.}) \quad ,(7)$$

The mass fraction of cellulose in wood may be estimated using the crystallinities of wood and cellulose:

$$\mathrm{cell.content} = \frac{\mathrm{Cr.I.}'}{\mathrm{Cr.I.}_{\mathrm{cell}}} \quad ,(8)$$

where: $\mathrm{Cr.I.}_{cell}$ = 70 %.[14]

Parameter	Sample: A	B	C
Cr.I.	0.49	0.46	0.41
Cr.I.'	0.48	0.42	0.29
L_{002} (nm)	3.62	3.67	3.78
X	0.47	0.47	0.49
O.I.	0.66	0.63	0.58
L.O.	22	19	8
Mesomorphism	0.18	0.21	0.29
Cellulose content	0.68	0.60	0.41

Table 3. The calculated values of several parameters estimated from the diffraction pattern for lime wood samples of different age.

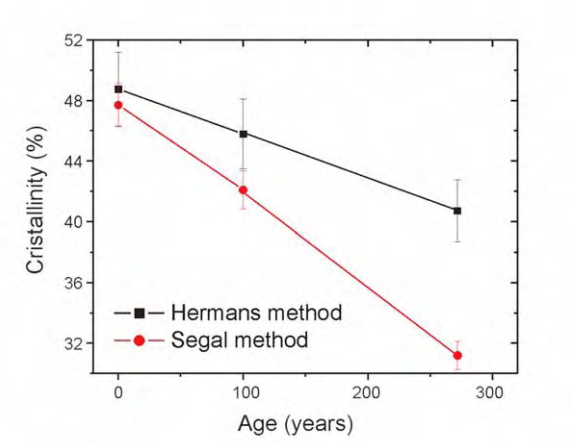

Figure 7. The fraction of crystalline material versus age of lime wood samples.

In Table 3 the calculated parameters for the studied wood samples are presented.

The uncertainties in crystallinity index determination are 5% (N = 3) and in the intensity ratio 3%. Almost all estimated values decrease with the sample age, while the apparent crystallite size, fraction of crystallite interior chains, and mesomorphism increase. An increase in structural disorder and degradation of the cellulose and hemicelluloses due to microbiological attack may explain the decrease of crystallinity with age. Lignin degrades at a slower rate, because of its aromatic structure and hence resistance to degradation. The linear decrease of the crystalline index of lime wood samples with increasing age is evident from Figure 7.

3.4 IR spectroscopic analyses

FT-IR spectroscopy if often used to characterize wood[2,21] and to determine lignin content in pulp, paper and wood. It has also been used for determination of chemical changes in wood during weathering, fungal decay,[22] and chemical treatments,[23] and its use was recently reviewed by Moore and Owen.[24] Two information-rich regions of the FT-IR spectra of the studied lime wood samples are shown in Figure 8.

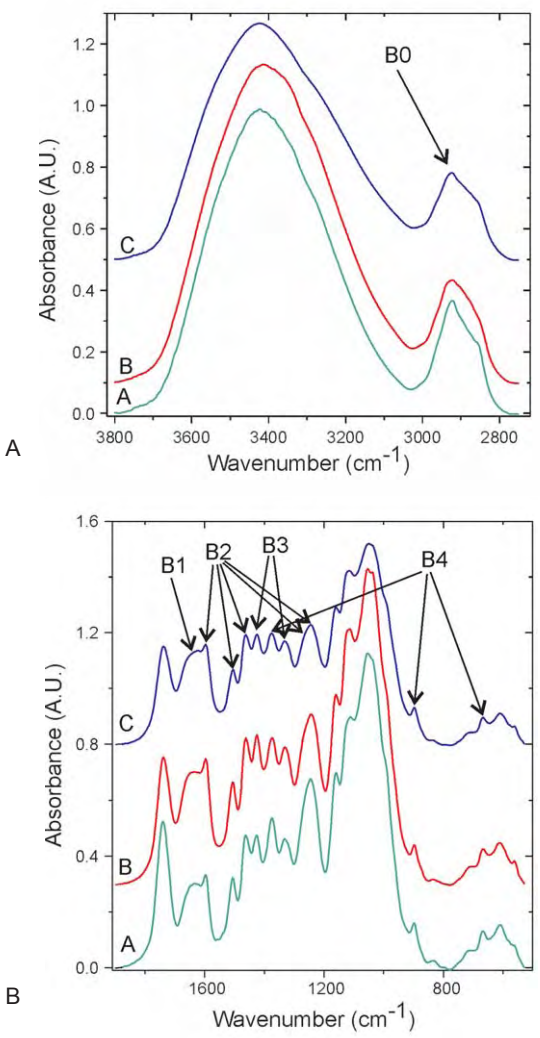

Figure 8. FT-IR spectra of lime wood samples under study: (a) 3820 - 2700 cm-1 region; (b) 1900 - 770 cm-1 region.

In Figure 8 the most representative bands, according to the literature,[7,8,23,26-35] are pointed out - B0: the asymmetric methoxyl C-H stretching; B1: absorbed water; B2: bands assigned to different lignin groups; B3: bands common to lignin and cellulose; B4: bands assigned to cellulose. Lignin exhibits significant absorbance also in the regions, which are usually used for cellulose crystallinity determination (particularly at 1426 cm^{-1} and 2855 cm^{-1}) so that lignin may interfere with cellulose crystallinity determination.

Generally, the secondary derivative of IR spectra can enhance the apparent resolution and amplify small differences. The second derivative spectra of the three lime wood samples are shown in Figure 9.

From the derivative FT-IR spectra of the samples several differences can be observed. The band at 1661 cm^{-1} decreases with increasing sample age while the band at 1634 cm^{-1}, which in the non-degraded sample appears like a shoulder,

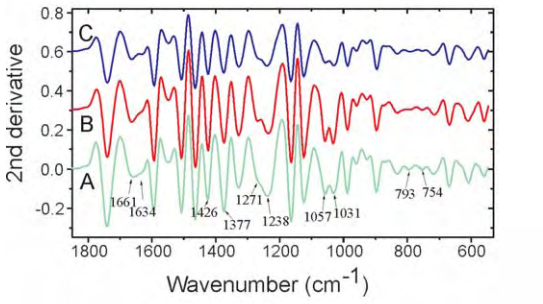

Figure 9. Second derivative FT-IR spectra of the lime wood samples.

becomes more prominent with increased age. This band is assigned to absorbed water; probably due to an increasingly oxidised surface, the absorption capacity of degraded wood also increases.

From the FT-IR spectra, similarly as from diffractograms, one can conclude that the relative lignin content increases, as it is more resistant to degradation under environmental conditions. Simultaneously, the band at 1377 cm^{-1} assigned to C-H bending in cellulose and hemicelluloses decreases with time.

Other bands which exhibit visible variations are at 1057 cm^{-1} and 1030 cm^{-1}, assigned to C-O stretching in C(3)-O(3)H bonds in cellulose and hemicelluloses. The disappearance of these bands is evident in aged lime wood of approx. 100 years. Also, the bands at 793 cm^{-1} and 754 cm^{-1} assigned to the cellulose ring vibrations become smaller with increased age.

For estimation of cellulose crystallinity on the basis of IR data, researchers use different absorption bands. The relative crystallinity index is usually defined as the ratio between intensities or integral absorptions of the following bands: 1100 to 690 cm^{-1};[36] also 1377 to 668 cm^{-1} (Cr.I.);[37] then 1426 to 895 cm^{-1} as the lateral order index (L.O.I.); and 1377 to 2921 cm^{-1} as the total crystallinity index (T.C.I.).[11,23,38]

Several crystallinity indices were calculated: in Figure 10, the crystallinity index, lateral order index and total crystallinity index are plotted against the age of samples. The average error was evaluated to be 5%. As evident from the data, the Cr.I. evaluated from the ratio of absorbances 1377 to 2920 cm^{-1} and 1377 to 668 cm^{-1} decrease with sample age, which correlates with XRD results.

The intensities of several IR absorption bands characteristic for cellulose were also compared to the intensity of the 1505 cm^{-1} band that is sometimes used as an internal standard assigned to benzene ring stretching of lignin, as it is more

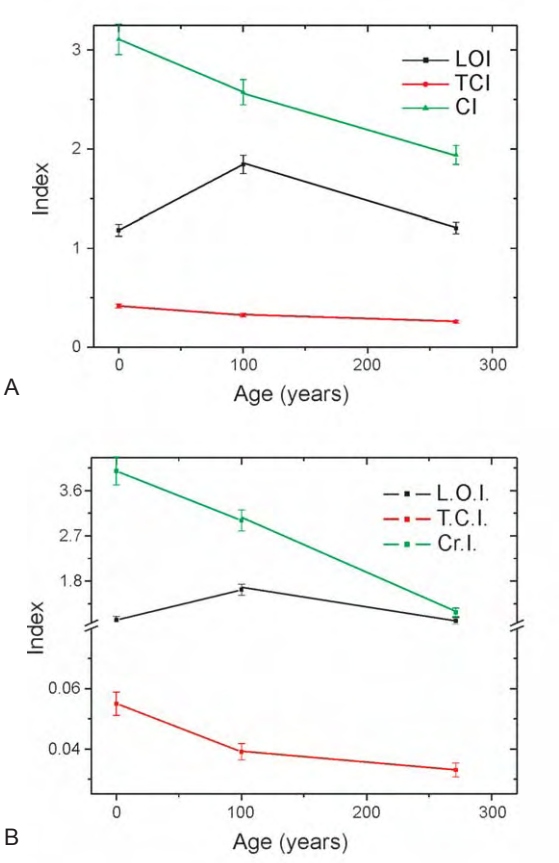

Figure 10. The relative crystallinity index calculated from different intensities ratios (a) and different integral absorbance ratios (b).

resistant to degradation and probably degrades at a lower rate (Table 4). The observed differences again indicate that carbohydrates degrade first, while after longer periods of degradation, lignin is also decomposed, possibly by a different microorganism.

3.5 2D correlation spectroscopy

By inspection of the synchronous and asynchronous spectra of the three samples, the sequence of variation could be estimated. The rules are as follows: if the cross peaks in synchronous spectrum (v_1, v_2) is positive (assuming that $v_1 > v_2$), and the cross peak at the same position in asynchronous spectrum is also positive, then the change at v_1 may occur prior to that of v_2. If the cross peak in asynchronous spectrum is negative, so the change at v_2 may occur prior to that of v_1. If the v_1, v_2 in synchronous spectra are negative, the rules are reversed. In the correlation spectra, the FT-IR spectrum of the non-degraded lime wood was considered as the reference.

In Figure 11 we show synchronous (a) and asynchronous (b) correlation spectra of lime wood samples in the 3700–2700 cm^{-1} region depending on the age of samples. In synchronous correlation spectra, two auto-peaks at 3415 cm^{-1} and 2920 cm^{-1} were found (Figure 11a). The first auto-peak indicates a significant variation with the sample age. A positive cross peak is observed at 3415 vs. 2920 cm^{-1}. Three negative cross peaks at 3415 vs. 3060 cm^{-1}, 3060 vs. 2920 cm^{-1}, and 3060 vs. 2860 cm^{-1} are observed, meaning that the intensities of these bands vary in the opposite directions (one increases while the other one decreases).

The asynchronous correlation spectra possess excellent deconvolution ability. In the spectral range 3700 cm^{-1} - 2700 cm^{-1} one can observe several cross peaks. The existence of three asynchronous cross-peaks 3623 cm^{-1} vs. 3430 cm^{-1}; 3430 cm^{-1} vs. 3353 cm^{-1}; and 3145 cm^{-1} vs. 3430 cm^{-1} indicates that the wide water vibration band in the spectral region 3000–3700 cm^{-1} is split into 4 separate bands located at around 3623, 3430, 3353 and 3145 cm^{-1}, which overlap in the 1D IR spectra. The two components at 3350 cm^{-1} and 3430 cm^{-1} are believed to correspond to the absorbance from the strongly hydrogen-bonded and less strongly hydrogen-bonded hydroxyl groups existing in liquid water, respectively. The 3623 cm^{-1} band could be due to a small population of weakly bonded water.

The sign of asynchronous correlation peak at $v_1 = v_2$ gives information about the sequential order of intensity changes between band v_1 and band v_2. According to Noda, if $v_1 > v_2$, and the sign of the asynchronous band at $v_1 = v_2$ is positive (solid line), band v_1 will vary prior to band v_2, while the negative asynchronous band (dashed line) implies opposite phenomena.

According to this rule, the positive asynchronous bands at 3623 cm^{-1} vs. 3430 cm^{-1} in the left upper triangle reveal that the change of population of the high wavenumber feature (3623 cm^{-1}) occurs earlier than the change of the population of the strongly hydrogen bonded OH-species (3430 cm^{-1}).; while the negative 3430 cm^{-1} vs. 3353 cm^{-1} and 3145 cm^{-1} vs. 3430 cm^{-1} bands suggests that the 3430 cm^{-1} and 3353 cm^{-1} bands vary prior to 3430 cm^{-1} and 3145 cm^{-1} bands.

Sample	I_{1505}/I_{1738}		I_{1505}/I_{1375}		I_{1505}/I_{1158}		I_{1505}/I_{895}	
	Height	Area	Height	Area	Height	Area	Height	Area
A	0.30	0.13	0.89	1.40	0.92	0.92	1.88	3.58
B	0.46	0.25	1.32	2.41	1.01	1.12	2.34	4.93
C	0.34	0.17	1.11	1.98	0.94	1.00	1.49	2.87

Table 4. Lignin/carbohydrate ratio calculated from FT-IR spectra.

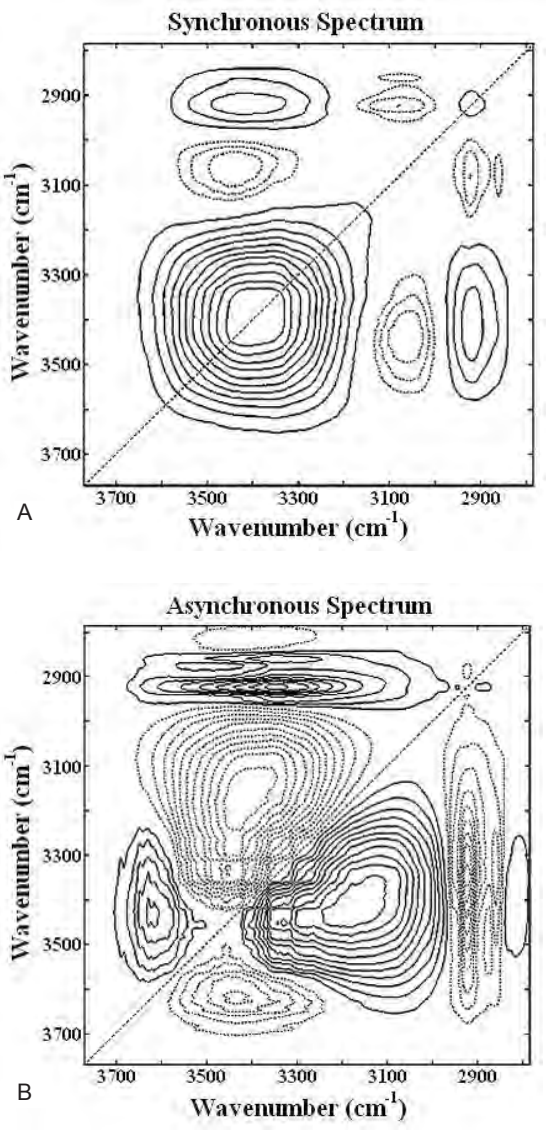

Figure 11. 2D correlation spectra, synchronous (a) and asynchronous (b) in the 3700-2700 cm-1 region of the lime wood samples. The variable is aging time. The FT-IR spectra of the samples of 100 and 300 year were reported to that of undegraded sample. Solid line: positive values, dashed line: negative values.

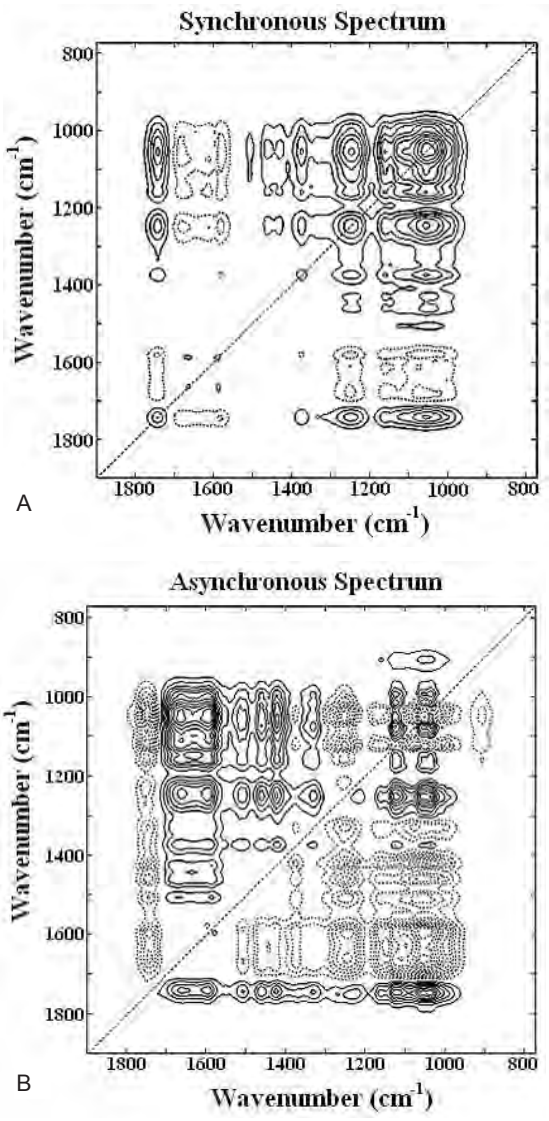

Figure 12. 2D correlation spectra, synchronous (a) and asynchronous (b) in the 1800-800 cm-1 region of the lime wood samples. The variable is aging time. The FT-IR spectra of the samples of 100 and 300 year were reported to that of undegraded sample. Solid line: positive values, dashed line: negative values.

In Figure 12 we present the synchronous and asynchronous 2D correlation spectra in the 1800-800 cm^{-1} region. In the synchronous spectra (Figure 12a) seven auto-peaks can be observed. The corresponding cross-peaks (off-diagonal peaks) are observed for all auto-peaks. Eighteen positive cross peaks are evident which vary simultaneously in the same direction. Nine negative cross peaks can also be noted.

In the correlation spectra it evident that the 1658 cm^{-1} band assigned to C=O stretching in conjugated p-substituted aryl ketones and/or absorbed water, is significant in the spectrum of sample B, and its intensity is higher also in the spectrum of the degraded wood 270 years old. Such evaluation allows us to investigate oxidative modifications in wood components during degradation in natural conditions, which are hardly evident in the 1D FT-IR spectra.

We have shown that the 1658 cm^{-1} band is very intense for all samples, yet decreasing in the sample order: B > C > A. Its changes are observed more easily than those of the band at 1465 cm^{-1} corresponding to O-H in-plane bending vibration in cellulose I, or C-H bending in lignin; or those of the band at 1426 cm^{-1} assigned to aromatic skeletal stretching and C-H in-plane bending in lignin and carbohydrates, or CH_2 sym-

metric scissoring in cellulose I; or those of the 1030 cm^{-1} band of C-O stretching mainly from C(3)-OH in cellulose I and hemicellulose which otherwise exhibit only a small variation (in the sample order B > A > C). The changes in these bands appear sooner than those of the bands at 1377 cm^{-1} corresponding to CH bending in cellulose and hemicellulose, at 1240 cm^{-1} of OH in-plane bending, C-C , C-O , C=O stretch in lignin and xylan; or at 1057 cm^{-1} assigned to C-O stretching mainly from C(3)-OH in cellulose I and hemicelluloses (in the sample order A > B > C).

As mentioned in the introduction, different kinds of fungi, bacteria and other microorganisms selectively degrade the wood components as carbohydrates, hemicellulose and lignin resulting in defibrillation and destruction of fibrils, specific structural changes of wood components, modification in crystallinity of cellulose, etc. These can be explained by several simultaneous and consecutive processes during lime wood degradation including oxidation, photo-oxidation, and biodegradation. This may lead to selective removal of a component such as cellulose and hemicelluloses, which results in increase of the relative content lignin and its degradation products. This was also demonstrated in this work for lime wood.

4. Conclusions

A description of morphological and compositional changes in lime wood from icons and iconostasis subjected to long-term degradation in environmental conditions was obtained using a variety of analytical methods. The information on specific features associated with different types of degradation of lime wood is important to plan appropriate conservation and specific consolidation procedures or other treatments.

X-ray diffraction and FT-IR provided evidence on the decrease of cellulose crystallinity and crystallite size. SEM revealed disruption of the fibrils and changes in their dimensions.

Qualitative and quantitative changes in lignin and carbohydrate components in wood were evaluated by FT-IR and it has been established that all bands assigned to carbohydrate compounds decrease with increased wood degradation state.

Investigations by 2D correlation analysis revealed complex phenomena associated with degradation, and allowed us to follow the changes over time. This lead to better understanding of the degradation phenomena in cultural heritage objects made of lime wood.

References

1. R. A. Blanchette, A review of microbial deterioration found in archaeological wood from different environments, Intern. Biodet. Biodegrad., 2000, **46,** 189-204.

2. X. Colom, F. Carrillo, F. Nogues, P. Garriga, *Structural analysis of photodegraded wood by means of FTIR spectroscopy*, Polym. Degrad. Stab., 2003, **80**, 543-549.

3. A. B. Strzelczyk, Observations on aesthetic and structural changes induced in Polish historic objects by microorganisms, Intern. Biodet. Biodegrad., 2004, **53** ,151-156.

4. I. C. A. Sandu, M. Brebu, C. Luca, I. Sandu, C. Vasile, *Thermogravimetric study on the ageing of lime wood supports of old paintings*, Polym. Degrad. Stab. 2003, **80**, 83-91.

5. I. C. A. Sandu, C. Luca, I. Sandu, P. Atyim, Research on the evaluation of degradation of softwood supports of old paintings with preparation layers I. Chemical composition and technical analysis (in Romanian), Rev. Chim. (Bucharest) 2001, **52**, 46-52; I. C. A. Sandu, C. Luca, I. Sandu, M. Pohontu, Research on the evaluation of degradation of softwood supports of old paintings with preparation layers II.IR and FTIR Spectroscopy (in Romanian), Rev. Chim. (Bucharest) 2001, **52**, 409-419.

6. I. Noda, Two-dimensional infrared spectroscopy of synthetic and biopolymers, Bull. Am. Phys. Soc., 1986, **31**, 520-528

7. I. Noda, Generalized two-dimensional correlation method applied to infrared, Raman, and other types of spectroscopy, Appl. Spectrosc., 1993, **47**, 1329-1336.

8. T. Nakano, S. Shimada, R. Saitoh, I. Noda, Transit 2D IR correlation spectroscopy of the photopolymerization of acrylic and epoxy monomers, Appl. Spectrosc., 1993, **47**, 1337-1342.

9. I. Noda, Two-dimensional infrared (2D IR) spectroscopy: Theory and applications, Appl. Spectrosc., 1990, **44**, 550-561.

10. A. A. Gorbushina, J. Heyrman, Th. Dornieden, M. Gonzalez-Delvalle, W. E. Krumbein, L. Laiz, K. Petersen, C. Saiz-Jimenez, J. Swings, *Bacterial and fungal diversity and biodeterioration problems in mural painting environments of St. Martins church (Greene–Kreiensen, Germany)*, Intern. Biodet. Biodegrad., 2004, **53**, 13-24.

11. N. Ghedini, C. Sabbioni, M. Pantani, *Thermal analysis in cultural heritage safeguard: an application*, Thermochim. Acta 2003, **406**, 105–113

12. R.H. Newman, "Estimation of the *lateral dimensions of cellulose crystallites using 13C NMR signal strengths*, Solid State Nucl. Magn. Res., 1999, **15**, 21-29.

13. N. E. Marcovich, M. M. Reboredo, M. I. Aranguren, *Modified woodflour as thermoset fillers. II. Thermal degradation of woodflours and composites*, Thermochim. Acta, 2001, **372**, 45-57.

14. B. L. Browning (Ed.), Encycl. Polym. Sci. Technol., "Wood", Vol. 15, John Wiley & Sons, New York, 1971, 1-40.

15. Y. Cao, H. Tan, *Study on crystal structures of enzyme-hydrolyzed cellulosic materials by X-ray diffraction*, Enzyme Microb. Technol., 2005, **36,** 314-317.

16. T. Heinze, T. Liebert, *Unconventional methods in cellulose functionalization*, Prog. Polym. Sci. 2001, **26**, 1689-1762.

17. Cr. I. Simionescu, M. Grigoras, A. Cernatescu-Asandei, Gh. Rozmarin, Physical methods in the study of poplar and some of its components, in Wood chemistry from Romania – the poplar and the willow trees, Romanian Academy, Bucharest, 1973, 107-149.

18. P. H. Hermans, J. J. Hermans, D. Vermaas, A. J. Weidinger, J. Polym. Sci, 1947, **3**, 1-7.

19. O. Ant-Wuorinen, O. A. Visapää, Pap. Puu, 1961, **49**, 207.

20. A. M. Donald, O. M. Astley, *Scattering Studies of Plant Cell Walls*, Mini-Reviews, 2002, 19-30, www.ccp13.ac.uk/fdr/2001/html/pdf/print/19.pdf (accessed 18/08/2005).

21. K. K. Pandey, *A study of chemical structure of soft and hard-wood and wood polymers by FTIR spectroscopy*, J. Appl. Polym. Sci. 1999, **71**, 1969–1975.

22. A. U. Ferraz, J. Baeza, J. Rodrigues, J. Freer, Estimating the chemical composition of biodegraded pine and eucalyptus wood by DRIFT spectroscopy and multivariate analysis, Biores. Technol. 2000, **74**, 201–212.

23. B. Interstosser, L. Salmen, *Application of dynamic 2D FTIR to cellulose*, Vibr. Spectr., 2000, **22**, 111-118.

24. F. Dadashian, W. A. Wilding, *Photodegradation of lyocell fibers through exposure to simulated sunlight*, Text. Res. J., 2001, **71**, 7-14.

25. A. K. Moore, N. L. Owen, *Infrared spectroscopic studies of solid wood*, Appl. Spectrosc. Rev., 2001, **36**, 65-86.

26. M. Schwanninger, J. C. Rodrigues, H. Pereira, B. Hinterstoisser, *Effects of short time vibratory ball milling on the shape of FT-IR spectra of wood and cellulose*, Vibrat. Spectrosc., 2004, **36**, 23-40.

27. T. Kondo, The assignment of IR absorption bands due to free hydroxyl groups in cellulose, Cellulose, 1997, **4**, 281-292.

28. L. J. Bellamy, *The Infra-red Spectra of Complex Molecules*, Chapman & Hall, London, 1975, 108-220.

29. K. Tashiro, M. Kobayashi, Theoretical evaluation of three-dimensional elastic constants of native and regenerated celluloses: role of hydrogen bonds**,** Polymer, 1991, **32**, 1516-1526.

30. C. Y. Liang, R. H. Marchessault, *Infrared spectra of crystalline polysaccharides. I. Hydrogen bonds in native celluloses***,** J. Polym. Sci., 1959, **37**, 385-395.

31. J. Sugiyama, J. Persson, H. Chanzy, Combined infrared and electron diffraction study of the polymorphism of native celluloses, Macromolecules, 1991, **24**, 2461-2466.

32. N. V. Ivanova, E. A. Korolenko, E. V. Korolik, R. G. Zbankov, Zh. Prikl. Spektroskop., 1989, **51**, 301-306

33. J. Mann, H. J. Marrinan, The reaction between cellulose and heavy water. Part 2. - Measurement of absolute accessibility and crystallinity, J. Chem. Soc., Farad, Trans. I, 1956, **52**, 487-492

34. K. K. Pandey, A. J. Pitman, *FTIR studies of the changes in wood chemistry following decay by brown-rot and white-rot fungi*, Intern. Biodeter. Biodegrad., 2003, **52**, 151-160.

35. F. Carrillo, X. Colom, J. J. Suńol, J. Saurina, *Structural FTIR analysis and thermal characterisation of lyocell and viscose-type fibres*, Eur. Polym. J., 2004, **40,** 2229-2234.

36. M. Ali, A. M. Emsley, H. Herman, R. J. Heywood, *Spectroscopic studies of the ageing of cellulosic paper*, Polymer, 2001, **42**, 2893-2900.

37. M. Akerholm, B. Hinterstoisser, L. Salmen, *Characterization of the crystalline structure of cellulose using static and dynamic FT-IR spectroscopy*, Carbohydr. Res., 2004, **399**, 569-578.

38. I. Noda, Y. Liu, Y. Ozaki, Two-Dimensional Correlation Spectroscopy Study of Temperature-Dependent Spectral Variations of N-Methylacetamide in the Pure Liquid State. 1. Two-Dimensional Infrared Analysis, J. Phys. Chem. 1996, **100,** 8665-8673.